Pure and Applied Geophysics

CrossMark

Gravity Maps of Antarctic Lithospheric Structure from Remote-Sensing and Seismic Data

ROBERT TENZER,[1] WENJIN CHEN,[2] ALEXEY BARANOV,[3,4] and MOHAMMAD BAGHERBANDI[5,6]

Abstract—Remote-sensing data from altimetry and gravity satellite missions combined with seismic information have been used to investigate the Earth's interior, particularly focusing on the lithospheric structure. In this study, we use the subglacial bedrock relief BEDMAP2, the global gravitational model GOCO05S, and the ETOPO1 topographic/bathymetric data, together with a newly developed (continental-scale) seismic crustal model for Antarctica to compile the free-air, Bouguer, and mantle gravity maps over this continent and surrounding oceanic areas. We then use these gravity maps to interpret the Antarctic crustal and uppermost mantle structure. We demonstrate that most of the gravity features seen in gravity maps could be explained by known lithospheric structures. The Bouguer gravity map reveals a contrast between the oceanic and continental crust which marks the extension of the Antarctic continental margins. The isostatic signature in this gravity map confirms deep and compact orogenic roots under the Gamburtsev Subglacial Mountains and more complex orogenic structures under Dronning Maud Land in East Antarctica. Whereas the Bouguer gravity map exhibits features which are closely spatially correlated with the crustal thickness, the mantle gravity map reveals mainly the gravitational signature of the uppermost mantle, which is superposed over a weaker (long-wavelength) signature of density heterogeneities distributed deeper in the mantle. In contrast to a relatively complex and segmented uppermost mantle structure of West Antarctica, the mantle gravity map confirmed a more uniform structure of the East Antarctic Craton. The most pronounced features in this gravity map are divergent tectonic margins along mid-oceanic ridges and continental rifts. Gravity lows at these locations indicate that a broad region of the West Antarctic Rift System continuously extends between the Atlantic–Indian and Pacific–Antarctic mid-oceanic ridges and it is possibly formed by two major fault segments. Gravity lows over the Transantarctic

Mountains confirms their non-collisional origin. Additionally, more localized gravity lows closely coincide with known locations of hotspots and volcanic regions (Marie Byrd Land, Balleny Islands, Mt. Erebus). Gravity lows also suggest a possible hotspot under the South Orkney Islands. However, this finding has to be further verified.

Key words: Antarctica, crust, gravity, lithosphere, upper mantle.

1. Introduction

The Antarctic tectonic plate structure has been of significant interest because of its unique tectonic and geological features. The current knowledge about the Antarctic geological and tectonic structure is, however, still limited due to a low spatial coverage of high-quality seismic data. To overcome this limiting factor, remote-sensing data observed by gravity and altimetry satellites could be used together with existing seismic information to interpret the Antarctic lithospheric structure.

Most of the seismic surveys in Antarctica have been conducted relatively recently, starting from the early 1960s. Existing studies include seismic data analysis done by Evison et al. (1960), Kovach and Press (1961), Bentley and Ostenso (1962), Dewart and Toksoz (1965), Adams (1971), Kogan (1972), Kolmakov et al. (1975), Knopoff and Vane (1978), Fedorov et al. (1982), Rouland et al. (1985), Ito and Ikami (1986), Rooney et al. (1987), Forsyth et al. (1987), Roult et al. (1994), Ritzwoller et al. (2001), Bannister et al. (2003), Winberry and Anandakrishnan (2004), Morelli and Danesi (2004), Reading (2006), Lawrence et al. (2006), Hansen et al. (2009), Baranov and Morelli (2013), Chaput et al. (2014), (An et al. 2015), and Ramirez et al. (2016). Since a lack of intra-plate seismicity in Antarctica (e.g., Okal

[1] Department of Land Surveying and Geo-Informatics, Hong Kong Polytechnic University, 181 Chatham Road South, Kowloon, Hong Kong, China. E-mail: robert.tenzer@polyu.edu.hk
[2] Department of Geodesy and Geomatics, Wuhan University, Wuhan, China.
[3] Schmidt Institute of Physics of the Earth, Russian Academy of Sciences, Moscow, Russian Federation.
[4] Institute of Earthquake Prediction Theory and Mathematical Geophysics, Russian Academy of Sciences, Moscow, Russian Federation.
[5] Division of Geodesy and Geoinformatics, Royal Institute of Technology (KTH), Stockholm, Sweden.
[6] Department of Industrial Development, IT and Land Management University of Gävle, Gävle, Sweden.

1981), passive seismic studies of earthquakes occurring mostly outside the Antarctic tectonic plate also represent a significant source of information about the Antarctic crustal structure. Some authors used the gravity, topographic, and ice-thickness information to interpolate the crustal structure where seismic data are missing. For more information, we refer readers to studies by Groushinsky et al. (1992), von Frese et al. (1999), Llubes et al. (2003), Studinger et al. (2004, 2006), Block et al. (2009), Jordan et al. (2010, 2013), Ferraccioli et al. (2011), Chaput et al. (2014), and (O'Donnell and Nyblade 2014).

A gravimetric interpretation of inner density structures utilizes methods for a forward modeling of the gravity and an inversion of the density (or the density interface). In principle, the information about the known density structure is used to compute the corresponding gravitational contribution that is subsequently removed from the observed gravity field. In this way, we could expose the gravitational signature of unknown (and sought) density structure or density interface. These methods were applied, for instance, by Tenzer et al. (2009a, 2015a) to interpret globally the gravitational signature of the oceanic lithosphere, isostatic signature of orogenic formations, and other major tectonic and geological features. In this study, we conducted a regional gravimetric interpretation of the Antarctic lithospheric structure based on the latest datasets of the gravity, topography, bathymetry, subglacial relief, sediment and crystalline crustal density structures, and Moho geometry. In particular, we used the BEDMAP2 subglacial relief (Fretwell et al. 2013), the GOCO05S gravitational field (Mayer-Gürr et al. 2015), and the ETOPO1 topographic and bathymetric dataset (Amante and Eakins 2009), together with the latest seismic crustal structure model for the Antarctic continent. This model was developed by Baranov et al. (2018) based on the results from the analysis of teleseismic receiver functions, seismic reflection and refraction data

(Molinari and Morelli, 2011), which were used to compile the ANTMoho model by Baranov and Morelli (2013), including results from processing the POLENET-ANET receiver functions (Chaput et al. 2014). This model includes also the oceanic crustal thickness estimated from gravity data. We used these datasets to compile the free-air, Bouguer, and mantle gravity maps over Antarctica and surrounding oceanic areas. We then used these gravity maps to interpret the Antarctic crustal and uppermost mantle structure, while focusing mainly on identifying the gravity pattern attributed to particular topographic, subglacial, and tectonic features. Here, we demonstrate that methods for interpreting the lithospheric structure based on combining information from seismic and remote-sensing data provide valuable information not only about known tectonic and geological features, but also could possibly indicate the existence of unknown features, especially in regions not covered sufficiently by seismic surveys. The subsequent part of the study is organized into five sections, starting with a brief review of methods for the gravimetric forward modeling in Sect. 2, which were applied in Sect. 3 to compile the refined gravity maps. We then present these results in Sect. 4, and interpret them in Sect. 5. Major findings are discussed and concluded in Sect. 6.

2. Methodology

We applied methods for a spherical harmonic analysis and synthesis of the gravity and crustal structure models to compute gravity corrections and refined gravity data corrected (step-wise) for all major known crustal density structures. The Bouguer gravity field obtained after applying this numerical procedure theoretically comprises mainly the gravitational signature of the Moho geometry. We then computed the mantle gravity field by applying an additional stripping gravity

correction to remove the Moho signature from the Bouguer gravity field to reveal the gravitational signature of the mantle. The spectral expressions used for the gravimetric forward modeling are summarized next.

2.1. Gravity Disturbances

For the external convergence domain $r \geq R$, the (free-air) gravity disturbance δg at a location (r, Ω) is computed from the coefficients $T_{n,m}$ of the disturbing potential T (i.e., difference between the actual and normal gravity potentials W and U respectively; $T = W - U$) as follows (e.g., Heiskanen and Moritz 1967).

$$\delta g(r, \Omega) = \frac{GM}{R^2} \sum_{n=0}^{\bar{n}} \sum_{m=-n}^{n} \left(\frac{R}{r}\right)^{n+2} (n+1) T_{n,m} Y_{n,m}(\Omega), \quad (1)$$

where $GM = 3986005 \times 10^8$ m^3 s^{-2} is the geocentric gravitational constant, $R = 6371 \times 10^3$ m is the Earth's mean radius, $Y_{n,m}$ are the surface spherical functions of degree n and order m, and $\bar{n}$ is the upper summation index of spherical harmonics. The 3-D position in Eq. (1) and thereafter is defined in the spherical coordinate system (r, Ω); where r is the radius, and $\Omega = (\varphi, \lambda)$ is the spherical direction with the spherical latitude φ and longitude λ.

2.2. Gravity Corrections

The gravity corrections were computed based on the method developed by Tenzer et al. (2009a) which utilizes the information about a 3-D density distribution within a particular geological unit, such as sedimentary basins (see also Tenzer et al. 2012a, 2012b, 2015a). The generic expression for a spherical harmonic synthesis reads

$$g(r, \Omega) = \frac{GM}{R^2} \sum_{n=0}^{\bar{n}} \sum_{m=-n}^{n} \left(\frac{R}{r}\right)^{n+2} (n+1) V_{n,m} Y_{n,m}(\Omega). \quad (2)$$

The potential coefficients $V_{n,m}$ of each volumetric mass layer are defined by.

$$V_{n,m} = \frac{3}{2n+1} \frac{1}{\bar{\rho}^{\text{Earth}}} \sum_{i=0}^{I} \left(Fl_{n,m}^{(i)} - Fu_{n,m}^{(i)} \right), \quad (3)$$

where $\bar{\rho}^{\text{Earth}} = 5500$ kg m^{-3} is the Earth's mean mass density, and the coefficients $\left\{ Fl_{n,m}^{(i)}, Fu_{n,m}^{(i)} : i = 0, 1, \ldots, I \right\}$ are defined as follows

$$Fl_{n,m}^{(i)} = \sum_{k=0}^{n+2} \binom{n+2}{k} \frac{(-1)^k}{k+1+i} \frac{L_{n,m}^{(k+1+i)}}{R^{k+1}}, Fu_{n,m}^{(i)}$$
$$= \sum_{k=0}^{n+2} \binom{n+2}{k} \frac{(-1)^k}{k+1+i} \frac{U_{n,m}^{(k+1+i)}}{R^{k+1}}. \quad (4)$$

The coefficients $\left\{ L_{n,m}^{(k+1+i)}, U_{n,m}^{(k+1+i)} : k = 0, 1, \ldots; i = 1, 2; n, m = 0, 1, \ldots, 180 \right\}$ in Eq. (4) describe the geometry and density (or density contrast) distribution within a particular volumetric mass layer. These coefficients are generated from discrete data (of depth, thickness, and density) using the following expressions for a spherical harmonic analysis (Tenzer et al. 2012a)

$$L_n^{(k+1+i)}(\Omega) = \begin{cases} \frac{2n+1}{4\pi} \iint\limits_{\Phi} \rho(D_U, \Omega') D_L^{k+1}(\Omega') P_n(t) \, d\Omega' \\ = \sum_{m=-n}^{n} L_{n,m}^{(k+1)} Y_{n,m}(\Omega) & i = 0 \\ \frac{2n+1}{4\pi} \iint\limits_{\Phi} \beta(\Omega') \alpha_i(\Omega') D_L^{k+1+i}(\Omega') P_n(t) \, d\Omega' \\ = \sum_{m=-n}^{n} L_{n,m}^{(k+1+i)} Y_{n,m}(\Omega) & i = 1, 2, \ldots, I \end{cases} \quad (5)$$

and

$$U_n^{(k+1+i)}(\Omega) = \begin{cases} \dfrac{2n+1}{4\pi} \iint\limits_{\Phi} \rho(D_U, \Omega') \, D_U^{k+1}(\Omega') P_n(t) \, \mathrm{d}\Omega' \\[2mm] \quad = \displaystyle\sum_{m=-n}^{n} U_{n,m}^{(k+1)} Y_{n,m}(\Omega) \qquad\qquad i = 0 \\[6mm] \dfrac{2n+1}{4\pi} \iint\limits_{\Phi} \beta(\Omega') \, \alpha_i(\Omega') \, D_U^{k+1+i}(\Omega') P_n(t) \, \mathrm{d}\Omega' \\[2mm] \quad = \displaystyle\sum_{m=-n}^{n} U_{n,m}^{(k+1+i)} Y_{n,m}(\Omega) \qquad\quad i = 1, 2, \ldots, I \end{cases} , \qquad (6)$$

where P_n are the Legendre polynomials for the argument t of cosine of the spherical angle ψ between two points (r, Ω) and (r', Ω'); i.e., $t = \cos\psi$. The infinitesimal surface element on the unit sphere is denoted as $\mathrm{d}\Omega' = \cos\varphi' \, \mathrm{d}\varphi' \, \mathrm{d}\lambda'$, and Φ is the full spatial angle. The integral convolutions in Eqs. (5) and (6) utilize a 3-D density distribution ρ defined by the following regression function.

$$\rho(r, \Omega) = \rho(D_U, \Omega) + \beta(\Omega) \sum_{i=1}^{I} \alpha_i(\Omega) \, (R - r)^i \quad \text{for}$$
$$R - D_U(\Omega) \geq r > R - D_L(\Omega),$$
$$(7)$$

where $\rho(D_U, \Omega)$ is a (nominal) value of the lateral density at a location Ω and at a depth D_U. The 3-D density contrast model with respect to the reference crustal density ρ^{ref} is defined as.

$$\Delta\rho(r, \Omega') = \rho(r, \Omega) - \rho^{\mathrm{ref}}, \qquad (8)$$

with $\rho(r, \Omega)$ given in Eq. (7).

2.3. Bouguer Gravity Disturbances

The Bouguer gravity disturbances δg^{cs} were computed from the (free-air) gravity disturbances δg after applying the topographic g^T and stripping gravity corrections due to density contrasts of the ocean (i.e., bathymetry) g^B, ice g^I, sediments g^S, and consolidated crust g^C to account for contributions of topography, bathymetry (offshore), continental glaciers, sedimentary basins (inland), marine sediments (offshore), and density heterogeneities within the crystalline crust. It is worth mentioning here that the atmospheric gravity correction is completely negligible in the context of this numerical study, because it reaches maxima less than 1 mGal (cf. Tenzer et al. 2009c). The computation was then realized according to the following scheme (Tenzer et al. 2009a).

$$\delta g^{cs} = \delta g - g^T - g^B - g^I - g^S - g^C. \qquad (9)$$

Tenzer et al. (2015a) demonstrated that the application of these gravity corrections yields the Bouguer gravity disturbances which have a high spatial correlation with the Moho geometry. These gravity data thus comprises mainly the Moho signature as well as the gravitational signal of mantle density heterogeneities (e.g., Tenzer et al. 2009a). However, these gravity data still comprise errors due to uncertainties of a crustal structure model used for computing the gravity corrections in Eq. (9).

2.4. Mantle Gravity Disturbances

To remove the Moho signature from the Bouguer gravity disturbances δg^{cs}, we applied the Moho stripping gravity correction g^M. This procedure yields the mantle gravity disturbances δg^m. Hence, we write.

$$\delta g^m = \delta g^{cs} - g^M, \qquad (10)$$

where g^M is defined by (cf. Tenzer et al. 2015a)

$$g^M(r, \Omega) = \frac{GM}{R^2} \sum_{n=0}^{\bar{n}} \left(\frac{R}{r}\right)^{n+2} \sum_{m=-n}^{n} F_{n,m}^M Y_{n,m}(\Omega).$$

(11)

The coefficients $F_{n,m}^M$ in Eq. (11), given by.

$$F_{n,m}^M = -\frac{3}{2n+1}\frac{n+1}{n+3}\frac{\Delta\rho^{c/m}}{\bar{\rho}^{\text{Earth}}} \sum_{k=1}^{n+3} \binom{n+3}{k} \frac{(-1)^k}{R^k} M_{n,m}^{(k)},$$

(12)

are defined for a constant value of the Moho density contrast $\Delta\rho^{c/m}$, which is chosen so that a minimum spatial correlation is attained between the mantle gravity disturbances and the Moho geometry (see also Tenzer et al. 2009a; 2012e; 2015a, 2015c). The Moho-depth coefficients $M_{n,m}$ and their higher-order terms $\{M_{n,m}^{(k)} : k = 2, 3, \ldots\}$ in Eq. (12) are generated from discrete values of the Moho depth D_M based on applying a discretization of the following integral convolution.

$$\sum_{m=-n}^{n} M_{n,m}^{(k)} Y_{n,m}(\Omega) = \frac{2n+1}{4\pi} \iint_{\Phi} D_M^k(\Omega') P_n(t) \, d\Omega'.$$

(13)

The mantle gravity disturbances δg^m comprise mainly the gravitational signal of the uppermost mantle, which is superposed over a weaker (long-wavelength) gravitational signal of density heterogeneities located deeper in the mantle. Obviously, errors due to uncertainties of Moho and crustal models propagate into these refined gravity data. The expected errors in these gravity data were discussed in detail by Tenzer et al. (2015a). Baranov et al. (2018) provided some error estimates in seismic data and their impact on gravimetric modeling and results.

3. Data Acquisitions

We used the new seismic crustal model (Baranov et al. 2018) with additional datasets to compute gravity corrections and refined gravity data according to the expressions given in Sect. 2. Input datasets and applied numerical procedures are briefly summarized next.

3.1. Input Datasets

We used the new seismic crustal model for the Antarctic continent developed by Baranov et al. (2018) for a gravimetric interpretation. This crustal model comprises three stratigraphic layers describing the sediment density distribution and three layers for the consolidated (crystalline) crust down to the Moho interface. The same concept was used before to construct the CRUST1.0 global seismic crustal model (Laske et al. 2013) in order to account for rather thick sediments and underlying consolidated crust, while the seismic velocity changes rapidly with depth. In addition to this model, we used the ETOPO1 topographic/bathymetric data and the BEDMAP2 subglacial relief to compute the gravity corrections, and the GOCO05S coefficients to generate the free-air gravity disturbances. The topography and subglacial bedrock relief in Antarctica are shown in Fig. 1. In Fig. 2, we plotted the glacial thickness, the total thickness of sediments and consolidated crust, and the Moho depth with a 1 × 1 arc-deg spatial resolution.

The Antarctic continent is almost entirely covered by continental glaciers (about 99%) with an average thickness of 1.94 km (Fretwell et al. 2013). Large parts of Antarctica are formed by subglacial sedimentary basins (Fig. 2b) of different properties and origin (Studinger et al. 2003; Bamber et al. 2006). In West Antarctica, most of large sedimentary basins are associated with the extensional tectonism of that region. In the Ross Sea regions, the largest sedimentary deposits are accumulated along the Victoria, Central, and Eastern basins with a thickness up to about 8 km (Trey et al. 1999). Sedimentary basins attributed to the continental crustal extension were formed also in Weddell Sea Embayment, with the largest sedimentary basin under the Filchner-Ronne Ice Shelf, with thickness variations from 2 to about 15 km (Huebscher et al. 1996; Leitchenkov and Kudryavtzev 1997). Sediment accumulations in the Bentley depression are about 4 km. Sediments between the Bentley depression and the Ross Ice Shelf vary in thickness between 1 and 2 km, and near the coast (Pine Island Glacier) are up to 2 km thick. Compared to West Antarctica, sedimentary basins in East Antarctica are much smaller. The sediment thickness in the Lambert Rift is about 2–6 km, and
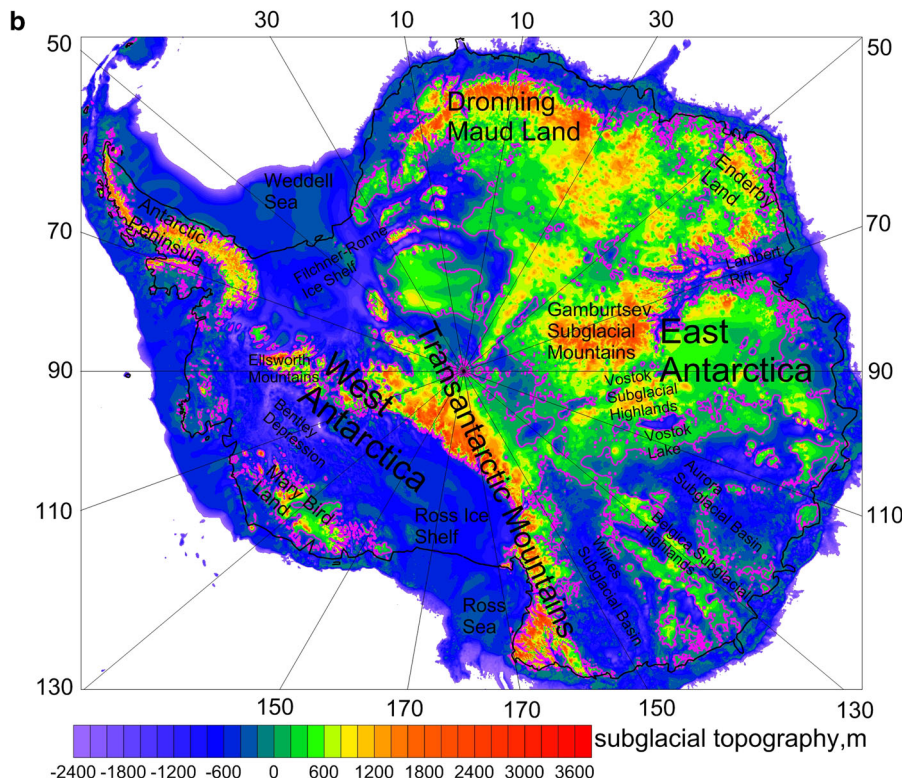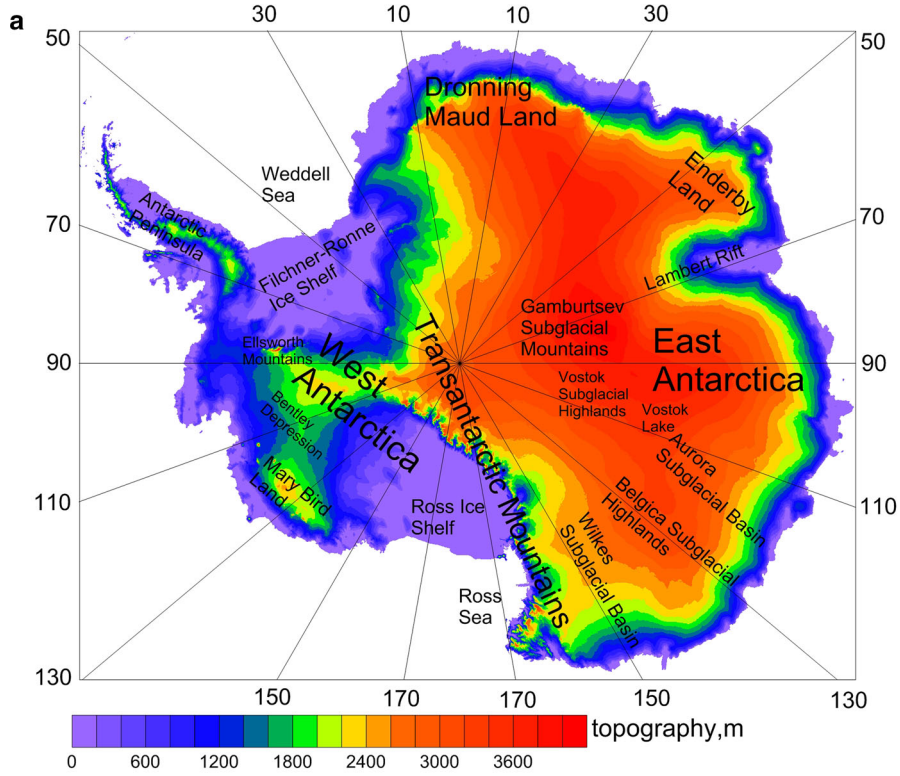
a topography, m

b subglacial topography, m

◄

about 2–4 km in the Vostok Basin. Sediments in the Wilkes Subglacial Basin, the Aurora Basin, and the Adventure Trough have a similar thickness of about 1 km.

As seen in Fig. 2c, the total thickness of the consolidated crust (i.e., the crustal thickness without the glacial and sediment covers) in Antarctica is relatively complex with large differences between the eastern and western Antarctica (Baranov et al. 2018). Except for the Antarctic Peninsula (30–38 km), the Marie Byrd Land (28–30 km), and the Ellsworth-Whitmore Mountains (32–34 km), they detected a thinned crust throughout the whole West Antarctica, with a different thickness of the consolidated crust under the Filchner-Ronne Ice Shelf (10–20 km), the Ross Ice Shelf (10–20 km), and the Bentley depression (16–20 km). They found a variable crustal structure under the Ross Sea, consisting of thin crustal sections of the Victoria Land (including the Central Basin) and the Eastern Basin that is separated by a thicker crust under the Central High. They also identified broad regions of extended crust of the Wilkes Subglacial Basin (26–30 km), the Lambert Rift (18–24 km), the Vostok Basin (24–28 km), and the Aurora Subglacial Basin (28–30 km) in East Antarctica. A thin consolidated crust under the Lambert Trench confirmed a potential boundary between three blocks (Indo-Antarctica, the central East Antarctic Craton and Australia) that once formed East Gondwana (Reading 2006). The largest crustal thickness was detected under the Gamburtsev Subglacial Mountains (56–58 km). In the Dronning Maud Land, a thick consolidated crust of the Wohlthat Massif (48–50 km) and the Kottas Mountains (48–50 km) is separated by a relatively thin crust along the Jutulstraumen Rift. Other regions of East Antarctica have a normal continental crust, with slightly different crustal thickness under the Enderby Land (36–40 km), the Prince Charles Mountains (34–40 km), the Princess Elizabeth Land

(34–38 km), the Belgica Subglacial Highlands (30–34 km), and the area of the South Pole (30–36 km). The Transantarctic Mountains have a normal continental crust (30–40 km), except for its central part with a thickened crust (40–46 km).

The Moho depth in Antarctica varies significantly (Fig. 2d) with minima detected in West Antarctica under the Ross Sea Ice Shelf (16–24 km) and the Bentley depression (20–22 km) and maxima under the Gamburtsev Subglacial Mountains (56–58 km) and the Dronning Maud Land (48–50 km). Except for the Antarctic Peninsula (34–38 km) and the Ellsworth-Whitmore Mountains (32–36 km), West Antarctica is characterized by a thin continental crust. Broad regions with a normal or slightly shallow Moho are seen in East Antarctica, particularly a rift between the western and central part of the Dronning Maud Land (30–34 km), the Enderby Land (38–42 km), the Lambert Rift (24–28 km), the South Pole region (32–36 km), the Prince Charles Mountains (34–40 km), the Princess Elizabeth Land (36–40 km), the Aurora Subglacial Basin (30–34 km), the Belgica Subglacial Highlands (34–36 km), and the Wilkes Subglacial Basin (30–34 km). The Transantarctic Mountains mostly have a normal Moho (34–38 km) except for its central part (40–46 km).

3.2. Numerical Procedures

We generated the gravity disturbances according to the equation in Eq. (1) from the GOCO05S coefficients. The normal gravity component was computed according to the GRS80 normal gravity parameters (Moritz 2000). We then computed the topographic and stripping gravity corrections due to anomalous crustal density structures (Eqs. 2–6) with the same spectral resolution and applied these corrections to the gravity disturbances (Eq. 9). The topographic gravity correction was computed using the ETOPO1 topographic data and adopting the average upper continental crustal density of 2670 kg m^{-3} (Hinze 2003). The same density value was used in definitions of density contrasts (Eq. 8) for computing the stripping gravity corrections. The bathymetric-stripping gravity correction was computed from the ETOPO1.0 bathymetric data. The
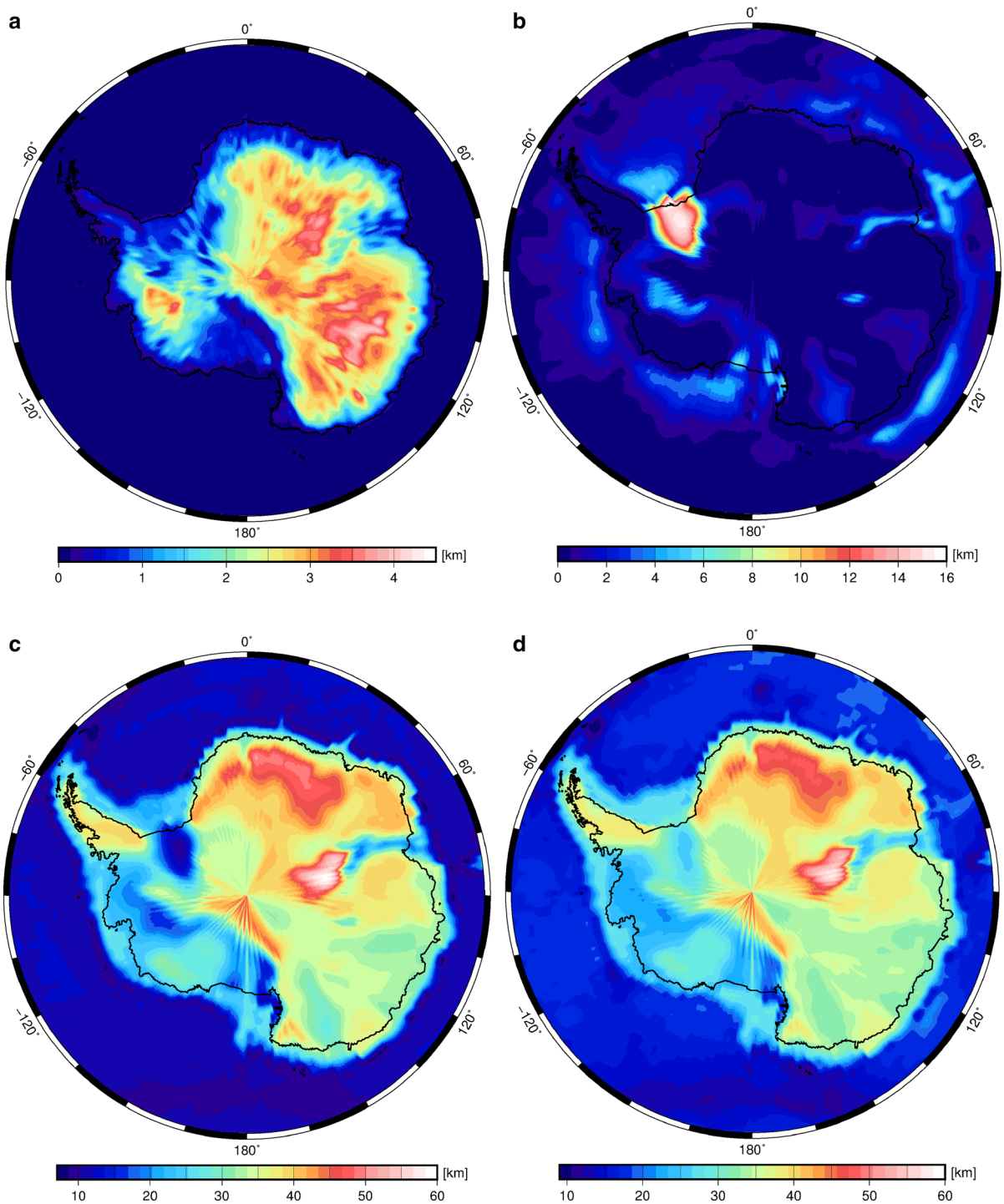
Figure 2
Maps of: **a** the ice thickness, **b** the sediment thickness, **c** the consolidated crustal thickness, and **d** the Moho depth. The ice cover at the Aurora Subglacial Basin reaches a maximum thickness of 4.6 km. The largest sediment accumulations are under the Filchner-Ronne Ice Shelf with a maximum thickness up to 15 km. The largest thickness of the consolidated crust (and the Moho depth) under the Gamburtsev Subglacial Mountains exceeds 50 km

ocean density contrast was evaluated for a depth-dependent seawater density model (Gladkikh and Tenzer 2011; see also Tenzer et al. 2011; 2012c). The ice-stripping gravity correction was computed from the ETOPO1.0 topographic data and the BEDMAP2 ice-thickness data and adopting the glacial density of 917 kg m^{-3} (Cutnell and Kenneth 1995). The sediment-stripping gravity correction was evaluated using the new seismic sediment model for Antarctica (Fig. 2b), the CRUST1.0 sediment data for continental sedimentary basins outside Antarctica, and a marine sediment density model developed by Tenzer and Gladkikh (2014) and Chen et al. (2014) to represent the density distribution within the marine sediments. The new seismic crustal model for Antarctica (Fig. 2c) and the CRUST1.0 data were used to compute the consolidated crust-stripping gravity correction. Finally, we computed the Moho stripping gravity correction (Eqs. 11–13), and the mantle gravity disturbances (Eq. 10). Here, we used again the Moho information from the new crustal model for Antarctica as well as from the CRUST1.0, because the computation of the Moho-depth coefficients $M_{n,m}$ in Eq. (13) requires a global integration. Moreover, we adopted a constant value of 480 kg m^{-3} for the Moho density contrast. As discussed by Baranov et al. (2018), the choice of a constant density contrast at the Moho interface is reasonable, because a spatial distribution of the Moho velocity changes in Antarctica is poorly constrained by the current distribution of passive seismic arrays.

4. Results

The gravity corrections computed according to numerical procedures described in Sect. 3 were applied here to compute the Bouguer gravity disturbances, and subsequently the mantle gravity disturbances. The gravity corrections and the refined gravity disturbances were computed at the topographic surface with a spectral resolution complete to the spherical harmonic degree of 180. For this purpose, we evaluated topographic heights of the computation points from the ETOPO1 topographic data with the same spectral resolution. All computations were realized on a 1 × 1 arc-deg grid of spherical coordinates within an area from the South Pole to the parallel 60 arc-deg of the southern latitude.

4.1. Gravity Corrections

The topographic gravity correction (Fig. 3a) has maxima over central parts of East Antarctica. The bathymetric-stripping gravity correction (Fig. 3b) reaches extreme values over deep oceans. The largest negative values of the ice-stripping correction (Fig. 3c) are seen in the central parts of East Antarctica, characterized by the largest glacial cover (Fig. 2a). The sediment-stripping gravity correction (for the upper layer) has extreme values along the continental margins of the Dronning Mauld Land and the Enderby Land in East Antarctica (Fig. 3d), reflecting large marine sediment deposits accumulated by a transport of terrigenous material to the marine environment by floating or grounded ice instead of fluvial processes (Wright and Anderson 1982). The maximum sediment thickness under the Filchner-Ronne Ice (Fig. 2b) propagates into large negative values of the sediment-stripping gravity correction attributed to deeper sediment sections (Fig. 3e, f). The consolidated crust-stripping gravity correction for the upper and middle layers (Fig. 3g, h) reaches maxima in West Antarctica over the Ellsworth-Whitmore Mountains, the Antarctic Peninsula, and the Dronning Maud Land. In East Antarctica, maxima of this correction over the central Gamburtsev Subglacial Mountains are detected only for the upper layer (Fig. 3g). Maximum values of this correction for the lower layer are along the continental margins of East Antarctica (Fig. 3i). Whereas the sediment-stripping gravity correction is everywhere negative, the consolidated crust-stripping gravity correction is typically positive (cf. Table 1). An opposite sign of these two stripping gravity corrections is explained by the fact that the sediment densities are below the chosen reference crustal density of 2670 kg m^{-3}, while the consolidated crustal densities typically exceed this value.
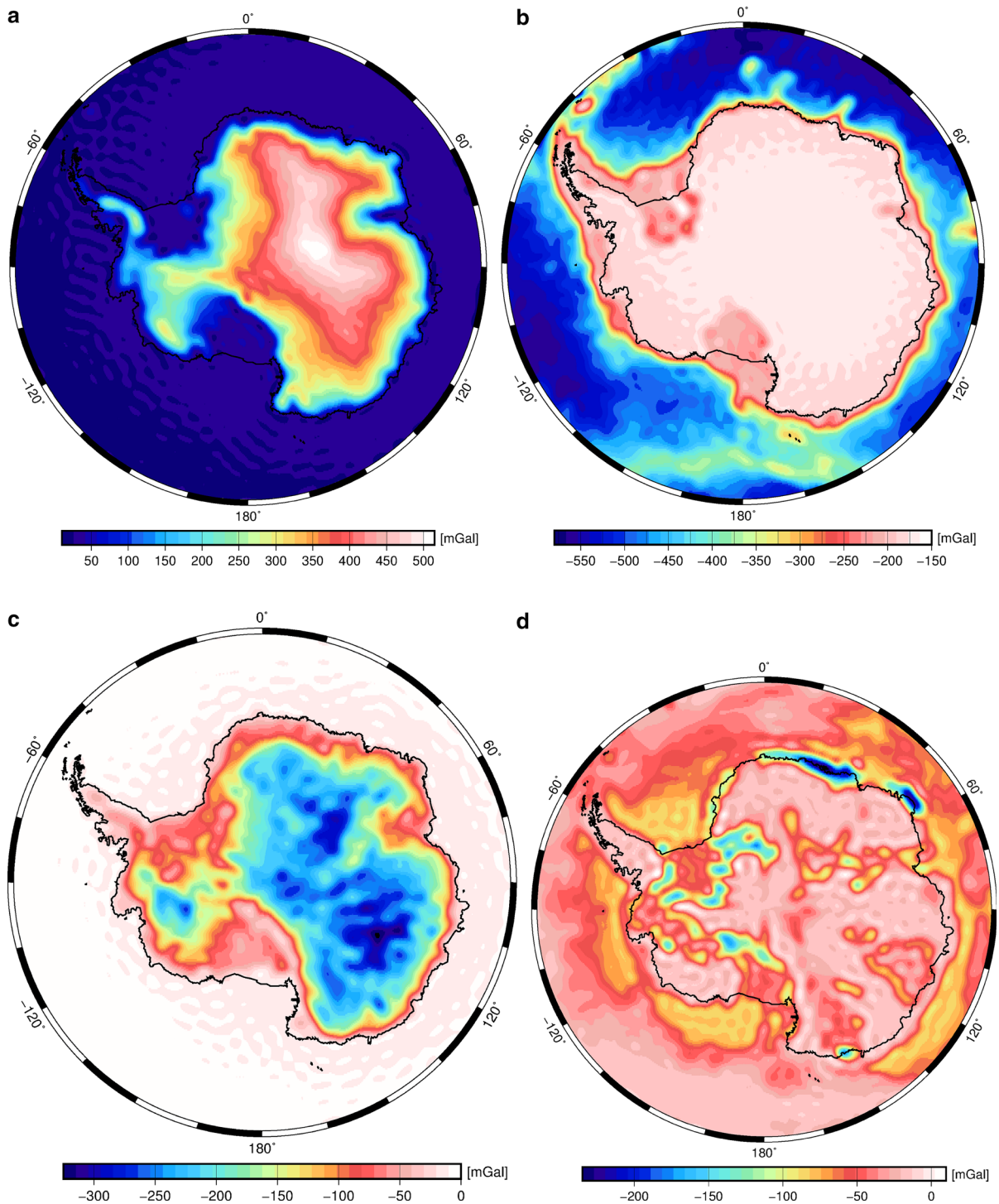
a

b

c

d

Figure 3

Gravity corrections: **a** topographic, **b** bathymetric, **c** ice, **d** upper, middle, and lower sediment, and **g–i** upper, middle, and lower consolidated crust. All gravity corrections were computed on a 1 × 1 arc-deg grid of surface points over Antarctica and surrounding oceans (from the South Pole to the parallel 60 arc-deg of the southern latitude) with the spectral resolution compete to the spherical harmonic degree 180

Figure 3
continued

Figure 3
continued

Table 1

Statistics of the gravity corrections (Fig. 3) computed on a 1 × 1 arc-deg grid of surface points over Antarctica and surrounding oceans (from the South Pole to the parallel 60 arc-deg of the southern latitude) with the spectral resolution compete to the spherical harmonic degree 180
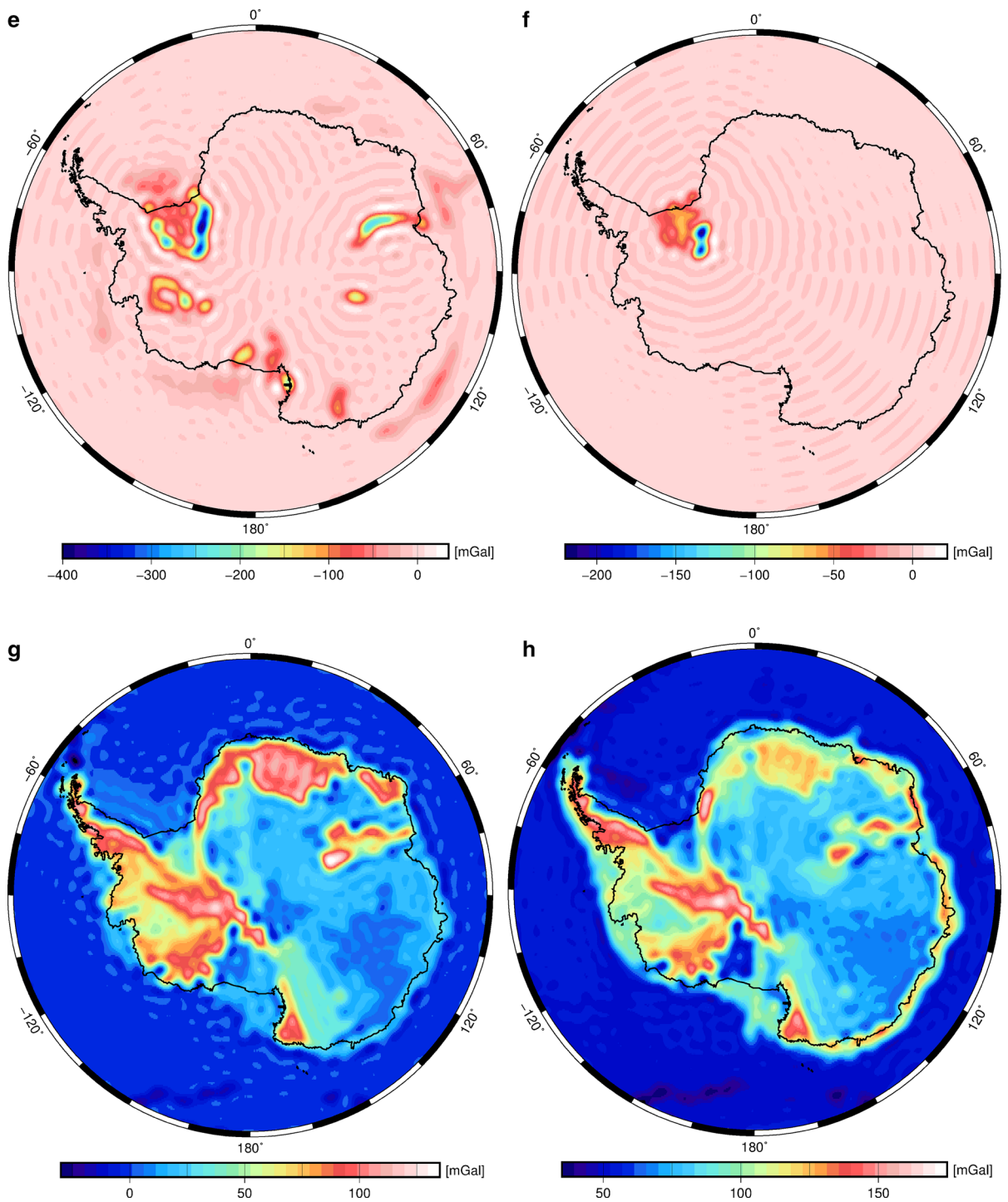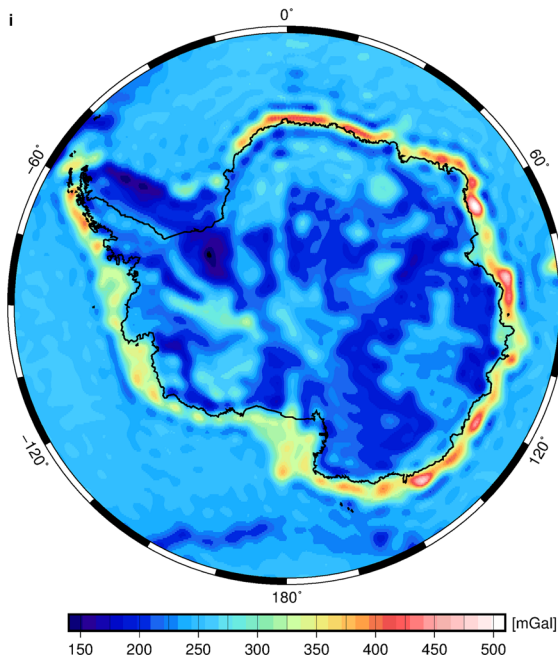
Gravity Correction	Min [mGal]	Max [mGal]	Mean [mGal]	STD [mGal]
Topographic	13	514	186	163
Bathymetric	− 575	− 157	− 272	138
Ice	− 325	− 5	− 107	97
Upper sediment	− 231	6	− 43	31
Middle sediment	− 397	34	− 12	32
Lower sediment	− 218	22	− 2	11
Upper crust	− 29	130	25	31
Middle crust	36	171	80	26
Lower crust	142	505	241	37

Note that the sediment- and crust-stripping gravity corrections were evaluated individually for the upper, middle, and lower layers

4.2. Bouguer Gravity Disturbances

The application of the topographic gravity correction substantially modified the gravity field inland (Fig. 4a), while the application of the bathymetric-stripping gravity correction mainly changed the gravity field offshore (Fig. 4b). The resulting gravity field obtained after applying these two gravity corrections is mostly negative inland and positive offshore. The application of the ice-stripping gravity correction reduced (in absolute sense) large negative gravity values inland (cf. Tenzer et al. 2010), while revealing to some extent the gravitational signature of subglacial bedrock topography (Fig. 4c). The sediment-stripping gravity correction enhanced the contrast between continental rifts and surrounding orogens, platforms, and shields (Fig. 4d) with the most pronounced changes in gravity maps over Filchner-Ronne Ice Shelf. We explain this by the fact that most of continental sediments infill continental rift zones. This result agrees with findings from a global study by Tenzer et al. (2015a). They demonstrated that the application of this correction enhanced the contrast between the oceanic and continental crustal structures, especially along continental margins with large accumulations of marine sediments mainly attributed to a river discharge. They also showed that the sediment-stripping gravity correction pronounced locations of continental basins. One example can be given over central Eurasia, where this correction significantly enhanced the contrast between the Himalayan–Tibetan Orogeny and the surrounding continental basins (Tarim, Qaidam, Sichuan, and Indo-Ganges) in the gravity field. The application of the consolidated crust-stripping gravity correction exhibited the contrast between the oceanic and continental crust along continental margins, revealed the isostatic signature of orogenic roots, and to a large extent exposed the Antarctic crustal thickness variations (Fig. 5). A more detailed interpretation of the Bouguer gravity map is postponed until Sect. 5.

4.3. Mantle Gravity Disturbances

Whereas the Bouguer gravity disturbances are positive as well as negative (Fig. 5, Table 2), the mantle gravity disturbances (Fig. 6) are only positive. Large variations in these gravity data (between 563 and 1780 mGal) are due to the uppermost mantle density structure as well as density heterogeneities deeper in the mantle (including the core–mantle boundary zone). The long-wavelength gravitational
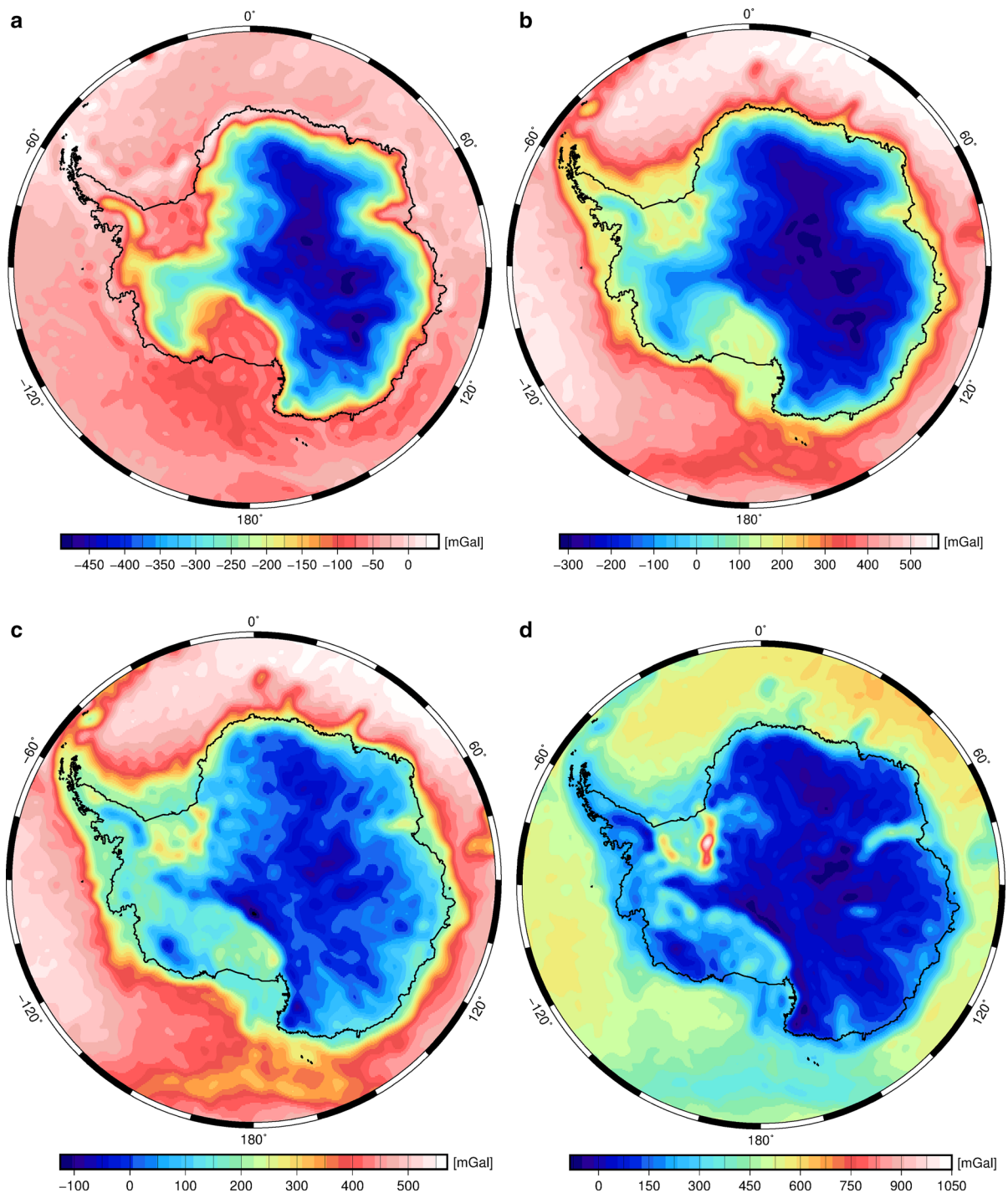
Figure 4

Regional gravity maps: **a** the topography-corrected gravity disturbances δg^T, **b** the topography-corrected and bathymetry-stripped gravity disturbances δg^{TB}, **c** the topography-corrected and bathymetry- and ice-stripped gravity disturbances δg^{TBI}, and **d** the topography-corrected and bathymetry-, ice- and sediment-stripped gravity disturbances δg^{TBIS}. All gravity values were computed on a 1×1 arc-deg grid of surface points over Antarctica and surrounding oceans (from the South Pole to the parallel 60 arc-deg of the southern latitude) with the spectral resolution complete to the spherical harmonic degree 180

Figure 5

Bouguer gravity disturbances δg^{cs} computed on a 1×1 arc-deg grid of surface points over Antarctica and surrounding oceans (from the South Pole to the parallel 60 arc-deg of the southern latitude) with the spectral resolution compl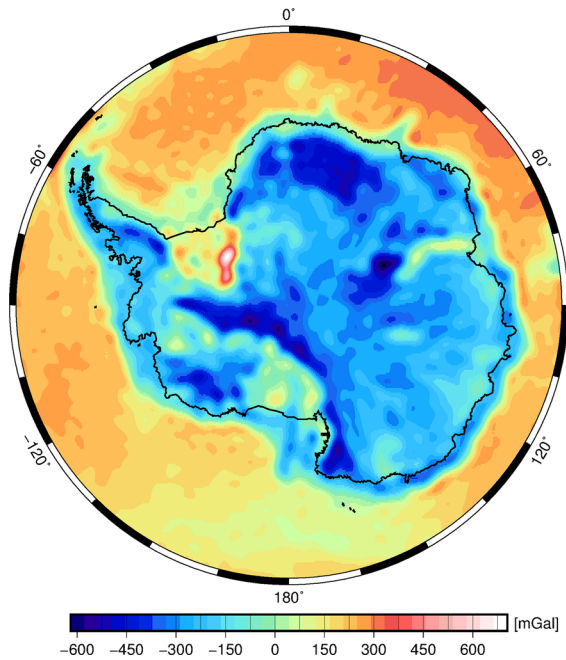ete to the spherical harmonic degree 180. Large negative values (in blue) are typically distributed over the continental crust (including continental margins) and positive values (in red) are over oceans
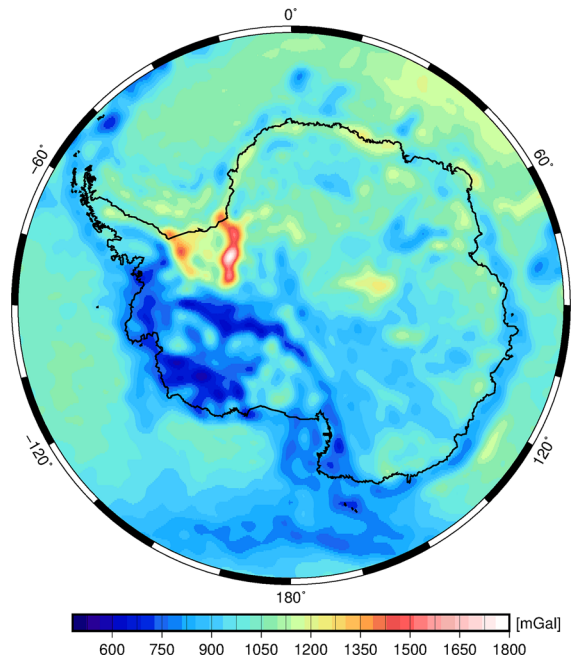
Table 2

Statistics of the free-air and (step-wise) corrected gravity disturbances computed on a 1×1 arc-deg grid of surface points over Antarctica and surrounding oceans (from the South Pole to the parallel 60 arc-deg of the southern latitude) with the spectral resolution compete to the spherical harmonic degree 180

Gravity Disturbances	Min [mGal]	Max [mGal]	Mean [mGal]	STD [mGal]
δg^{T}	− 86	84	− 13	27
δg^{T}	− 489	43	− 199	162
δg^{TB}	− 319	562	74	277
δg^{TBI}	− 123	569	181	192
δg^{TBIS}	− 82	1040	238	207
δg^{cs}	− 617	704	− 107	238

For the used notation see legends in Figs. 4 and 5

features mainly reflect the global mantle convection pattern. Most of the medium–higher degree gravitational spectrum comprises a signature of the subcrustal lithospheric structure, attributed to mantle upwelling currents (along extensional tectonic margins), subductions, or crustal load.

Figure 6

Mantle gravity disturbances computed on a 1×1 arc-deg grid of surface points over Antarctica and surrounding oceans (from the south pole to the parallel 60 arc-deg of the southern latitude) with the spectral resolution complete to the spherical harmonic degree 180. Gravity lows (in blue) are seen mainly along the West Antarctic Rift System, and gravity highs (in red) mark the margins of the Filchner-Ronne Ice Shelf

4.4. Global Gravity Pattern

As seen from these results, the free-air, Bouguer, and mantle gravity disturbances differ significantly. From a point of view of tectonic or geological structures affecting the density distribution and consequently the gravity field, we could roughly categorize specific gravity features as follows. The compressional tectonism responsible for a formation of orogens is manifested in the free-air gravity map by large positive values which are also highly spatially correlated with the topography. These positive gravity values are often coupled by negative values along continent–continent collision zones on the side of the subducted continental lithosphere. The extensional tectonism along mid-oceanic rift zones and continental basins propagates into negative gravity values. The overall pattern of the free-air gravity disturbances indicates the isostatic balance of large–medium-scale lithospheric features, while

extreme gravity values mostly agree with locations of isostatically uncompensated structures, such as oceanic subductions or more detailed topographic features. Volcanic island arcs are characterized by positive gravity values over islands and seamounts, coupled with negative gravity values around these islands. This regional isostatic signature around volcanic islands is attributed to a lithospheric flexure due to a volcanic load.

In the Bouguer gravity map, the compressional tectonism is manifested by large negative values over orogens, revealing the isostatic signature. Moreover, this gravity map exhibits the contrast between different thickness of the oceanic and continental crust with typically positive gravity values over oceans and negative gravity values inland. The Bouguer gravity field is, thus, closely spatially correlated with the crustal thickness (Tenzer et al. 2009b).

In the mantle gravity map, the divergent tectonic margins and hotspots are manifested by gravity lows. Tenzer et al. (2012d) also demonstrated that a density change attributed to a thermal state of the oceanic lithosphere is detectable in the mantle gravity field (see also Tenzer et al. 2015b, 2016). Gravity lows apply along mid-oceanic rifts, while the gravity increases with the age of the oceanic lithosphere. These spatial gravity variations over oceanic areas are explained by a conductive cooling and thermal contraction of the oceanic lithosphere. Moreover, a thermal lithospheric contraction is isostatically compensated by the ocean deepening. The largest spatial gravity variations across the oceanic divergent tectonic plate boundaries reflect the highest rates of increasing density, and consequently gravity, at the earliest stage of forming the oceanic lithosphere. The signature of compressional tectonism over orogens is, on the other hand, typically not manifested in this gravity map. In overall, the spatial pattern in the mantle gravity field mainly reflects a thermal state of the lithosphere, rather than particular tectonic features.

5. Interpretation of Results

In this section, we have interpreted gravity maps with respect to major known geological and tectonic features of the Antarctic tectonic plate.

5.1. Free-air Gravity Map

The free-air gravity disturbances in Antarctica vary mostly within ± 80 mGal (Fig. 7 and Table 2). This relatively small gravity interval indicates that most of the long–medium topographic features as well as lithospheric density heterogeneities are in isostatic equilibrium (aside from the signature of glacial isostatic adjustment). Gravity highs are distributed over the Antarctic Peninsula and large elevated parts of East Antarctica. Gravity lows are seen mainly along the West Antarctic Rift System and large parts of West Antarctica, including the Transantarctic Mountains. This finding supports theories of a non-collisional origin of the Transantarctic Mountains (ten Brink et al. 1997), with no evidence of a compressional origin, thus different from most mountain ranges of a similar size (Studinger et al. 2004). A more detailed gravity interpretation of the Transantarctic Mountains is postponed until Sect. 5.3.
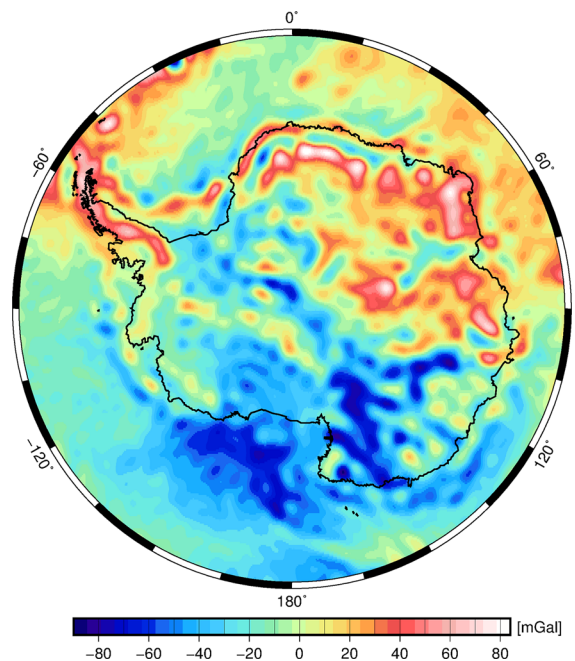

Figure 7

Free-air gravity disturbances δg computed on a 1×1 arc-deg grid of surface points over Antarctica and surrounding oceans (from the South Pole to the parallel 60 arc-deg of the southern latitude) using the GOCO05S coefficients complete to the spherical harmonic degree 180. Gravity highs are distributed over large parts of East Antarctica and Antarctic Peninsula

5.2. Bouguer Gravity Map

The Bouguer gravity disturbances in Antarctica vary significantly, with most of values distributed within the interval of ±600 mGal (Fig. 5 and Table 2). The most prominent feature in this gravity map is the contrast between the oceanic and continental crustal structure. This gravity pattern is associated with a different thickness of the oceanic and continental crust. Positive gravity values, mostly within a relatively small interval between 150 and 300 mGal, over open oceans reflect a thin and relatively uniform oceanic crustal thickness. Large horizontal spatial gravity changes along the Antarctic continental margins reflect a continental crustal thickening, while inland we also observe large gravity variations mostly within the interval of negative values. The largest negative gravity values are over mountains or subglacial mountains with deep orogenic roots. This gravity pattern confirmed a high spatial correlation between the Bouguer gravity field and the crustal thickness. These findings agree with a global pattern of the Bouguer gravity disturbances discussed in Sect. 4.4. Such gravity pattern could obviously be used to identify some major tectonic and geological features, such as the Antarctic continental margins. As seen in Fig. 5, the maximum continental extension offshore is along both sides of the West Antarctic Rift System between the Ross Sea Embayment and the Weddell Sea Embayment, both having an extremely thin continental crust. This is reflected in relatively small positive as well as negative gravity values (mostly within the interval ±150 mGal) over these areas, except for some large positive gravity values over parts of the Filchner-Ronne Ice Shelf. This region on the border of East Antarctic craton has very large positive gravity values (450–600 mGal) which are correlated with deep subglacial areas on the southern flank of the Filchner-Ronne Ice Shelf and may indicate the presence of relict oceanic crust. Nevertheless, such large positive gravity values are possibly overestimated due to systematic errors in the sediment density model. Other parts of the Filchner-Ronne Ice Shelf also have large positive gravity values which is consistent with a high degree of crustal extension there with anomalous mafic intrusion in the lower crust. Areas with moderate positive gravity values further extend along most of the West Antarctic Rift System, characterized again by a thin continental crust. Contours of this gravity pattern distinctively separate regions of the Filchner-Ronne Ice Shelf, the Bentley Depression, and the Ross Sea Shelf.

In contrast to these small and mostly positive gravity values, large negative gravity values prevail along the Transantarctic Mountains and the Ellsworth-Whitmore Mountains, both having a normal continental crust, except for the central part of the Transantarctic Mountains with a thickened crust. In West Antarctica, large negative gravity values are seen also over the Antarctic Peninsula and the Marie Byrd Land. The Antarctic Peninsula is very clearly separated by a deep subglacial depression from the Ellsworth-Whitmore Mountains, despite some structural similarities in their geology; see also (Behrendt et al. 1991). In East Antarctica, the largest negative gravity values mark the location of the Gamburtsev Subglacial Mountains, characterized by a young Alpine-age topography (Fretwell et al. 2013) and the maximum Moho deepening in Antarctica. Moreover, the gravity pattern there indicates relatively compact orogenic roots. Large negative gravity values are also detected over the Dronning Maud Land, Enderby Land, and the Prince Charles Mountains. The isostatic signature in the Bouguer gravity map in the case of the Dronning Maud Land indicates two or more localized orogenic roots, particularly under the Wohlthat Massif and the Kottas Mountains. These orogens are separated by Jutulstraumen Rift. Large localized negative gravity values are also seen over the Coats Land, but there is no confirmed evidence of orogenic roots. This complex pattern is explained by the fact that the Dronning Maud Land encompasses several crustal blocks, ranging in age from the Archean to the Early Paleozoic. The western part of the Dronning Maud Land includes the Archean Grunehogna Craton and the Grenville-age Maud Province (Jacobs et al. 1998). The Grunehogna Craton consists of the Archean granitic gneisses and the Mesoproterozoic sedimentary rocks (Groenewald et al. 1991). The Kottas Mountains have been interpreted as a remnant of an island arc. The Central Dronning Maud Land with the Wohlthat Massif is

associated with the Pan-African Orogeny during the assembly of Gondwana about 500–600 Myr (Jacobs et al. 2003). In contrast to these large negative gravity values, the Jutulstraumen Rift has a normal continental crust, marked by smaller negative gravity values. This rift represents a tectonic margin between the Grunehogna cratonic fragment and the late Neoproterozoic to Cambrian East African Antarctic Orogen (Marschall et al. 2013; Mieth and Jokat 2014; Jacobs et al. 2015).

The most pronounced contrast between gravity lows and highs in the Bouguer gravity map is seen between the Gamburtsev Subglacial Mountains (gravity lows) and the Lambert Rift (gravity highs). Elsewhere in East Antarctica, the gravity pattern appears to be more uniform, except for some small localized gravity variations which to some extent resemble a normal continental crust, with slightly different crustal thickness under the Enderby Land, the Prince Charles Mountains, the Princess Elizabeth Land, the Belgica Subglacial Highlands, and the area of the South Pole. We could also recognize some gravity features which agree with locations of the Vostok Subglacial Highlands and the Lake Vostok.

5.3. Mantle Gravity Map

A highly spatially correlated gravity pattern with the crustal thickness, seen in the Bouguer gravity map (Fig. 5), is absent in the mantle gravity map (Fig. 6). The only similarities in these two gravity maps are gravity lows along the Transantarctic Mountains, the Ellsworth-Whitmore Mountains, and the Marie Byrd Land. Moreover, the isostatic signature of orogens over the Dronning Maud Land and the Gamburtsev Subglacial Mountains is absent in the mantle gravity map. This is explained by removing the Moho signature from the mantle gravity data. The orogenic formations are typically characterized by large positive values of the free-air gravity disturbances as well as large negative values of the Bouguer gravity disturbances. A seen in Fig. 7, large positive values in the free-air gravity map are absent, except for the Gamburtsev Subglacial Mountains.

On the other hand, large negative values in the Bouguer gravity map (Fig. 5) are detected not only over the Gamburtsev Subglacial Mountains, but also over the Transantarctic Mountains, the Ellsworth-Whitmore Mountains, the Antarctic Peninsula, the Prince Charles Mountains, and the Marie Byrd Land. Moreover, a prevailing gravity pattern does not change significantly after removing the Moho signature. Gravity lows in the Bouguer gravity maps over the Transantarctic Mountains, the Ellsworth-Whitmore Mountains, and the Marie Byrd Land are seen again in the mantle gravity map. On the other hand, such situation does not repeat over the Dronning Maud Land and the Gamburtsev Subglacial Mountains, where gravity lows (present in the Bouguer gravity map) are absent in the mantle gravity map. These findings again confirmed a different origin of these geological formations; the one linked to the compressional tectonism that resulted in forming orogens (the Gamburtsev Subglacial Mountains and the Dronning Maud Land), while the other likely associated with the extensional tectonism along the West Antarctic Rift System (the Transantarctic Mountains, the Ellsworth-Whitmore Mountains, and the Marie Byrd Land).

We could also see a principal difference between the Ross Sea Ice Shelf and of the Filchner-Ronne Ice Shelf. The Ross Sea Ice Shelf has moderate negative values, while large areas of the Filchner-Ronne Ice Shelf have strong positive values up to about 1800 mGal and the maxima of positive values are related with deep trenches on the borders between the Filchner-Ronne Ice Shelf and the Ellsworth-Whitmore Mountains; also the highest positive values are observed on the border between the Filchner-Ronne Ice Shelf and the East Antarctic Craton.

Several theories have been proposed to explain possible mechanisms of forming the Transantarctic Mountains. Stern and ten Brink (1989) suggested that the heat conduction from the hot lithosphere of West Antarctica to East Antarctica and the isostatic response to erosion were the principal driving mechanisms behind the uplift of the Transantarctic Mountains. More recent models have included thermal buoyancy from an underlying positive temperature anomaly in the upper mantle (ten Brink et al. 1997), thicker crust giving the origin to an isostatically buoyant load (Studinger et al. 2004), or possible collapse of a high-standing plateau with the subsequent uplift and denudation (Bialas et al. 2007).

Models based on integrated geophysical analysis assumed that multiple mechanisms have contributed to the uplift of the Transantarctic Mountains (cf. Lawrence et al. 2006). Alternative hypotheses explaining this crustal feature suggest the continental rifting (Ferraccioli et al. 2011). According to Lawrence et al. (2007), the Late Cretaceous was characterized by the main phase of extensional tectonism between East and West Antarctica. The propagation southward of seafloor spreading from the Adare Trough into the continental crust underlying the western Ross Sea in the Early Cenozoic, likely caused a flexural uplift of the East Antarctic lithosphere, followed by a formation of the Transantarctic Mountains. It is worth mentioning here that the flexural uplift is not typically associated with rift flank uplift (typically characterized by a crustal thickening and subduction), but in the case of the Transantarctic Mountains it occurs at the same lithospheric boundary in conjunction with thermal expansion of the mountain belt, resulting in a very rapid surface uplift.

Gravity lows along the West Antarctic Rift System (except for Filchner-Ronne Ice Shelf), the Transantarctic Mountains, the Ellsworth-Whitmore Mountains and most of West Antarctica represent the most pronounced feature in the mantle gravity map. We could also see that gravity lows along the West Antarctic Rift System continuously extend towards the Atlantic–Indian Ridge and the Pacific–Antarctic Ridge. Moreover, this gravity pattern indicates the existence of two (almost parallel) rift zones (segments). The eastern continental segment roughly separates the Ross Sea Shelf and the Bentley depression from the Transantarctic Mountains and the Ellsworth-Whitmore Mountains, and then continues approximately between the Antarctic Peninsula and the Filchner-Ronne Ice Shelf. We would also see that—on the side of the Ross Sea—this segment likely comprises the Mt. Erebus volcanic region, extends offshore towards the Balleny Islands, and further to the Atlantic–Indian Ridge. The west (continental margin) segment is located along the continental margins of the Marie Byrd Land and the Antarctic Peninsula, and might include also a possible hotspot under the Marie Byrd Land. These two segments converge towards the north of the Antarctic

Peninsula, roughly around or under the South Orkney Islands, and further extend towards the Pacific–Antarctic Ridge. The presence of these gravity lows is explained by a low density of hot mantle along divergent tectonic margins and likely also hotspots and volcanic regions. A possible existence of hotspot under the Marie Byrd Land has been suggested in a number of studies. Winberry and Anandakrishnan (2004) reported, based on broadband seismic experiment, that the 25-km-thick crust measured on the southern flank of the Marie Byrd Land dome suggests that the high topography there is partially supported by a low-density mantle, possibly a hotspot. In contrast, the interior of the rift appears to be underlain by an average-density mantle, suggesting that active volcanism is not present beneath the interior of the West Antarctic Ice Sheet. The fact that a crustal thickness of only 21 km was measured in the Bentley subglacial trench suggests that the region has undergone locally extreme extension. According to a more recent study by Lloyd et al. (2015), the slowest relative P and S wave velocity anomaly observed extending to at least 200 km depth beneath the Executive Committee Range in the Marie Byrd Land indicates a warm, possibly plume-related, upper mantle with low seismic velocities (e.g., Accardo et al. 2014). They also stated that the detected low-velocity anomaly and inferred thermal perturbation (about 150 K) are sufficient to support isostatically the anomalous long-wavelength topography of the Marie Byrd Land, relative to the adjacent West Antarctic Rift System.

Despite most of the West Antarctic Rift System, including the Transantarctic Mountains, the Ellsworth-Whitmore Mountains, and the Marie Byrd Land are characterized by gravity lows, while the margins of the Filchner-Ronne Ice Shelf are marked by gravity highs with the most pronounced signature of the Dufek Massive. Since these gravity highs indicate large densities, their existence might be explained by a large gabbronic intrusion known as the Dufek intrusion, which is part of an extensive, Middle Jurassic igneous province that was related to, and emplaced just prior to Gondwana break-up. From magnetic data interpretations, Ferris et al. (1998) suggested that the emplacement of both phases of the Dufek intrusion was preceded by a period of

extensional block faulting which uplifted the Berkner Island basement block, and was succeeded by a further period of extensional faulting involving a component of strike-slip deformation during the initial stages of Gondwana break-up. Nevertheless, it is unlikely that a gabbronic intrusion could generate such large gravity anomalies (400–500 mGal). Instead, closer inspection of the sediment-stripping gravity corrections (see Figs. 3d–f) indicates that this gravity signature is also affected by errors in the used sediment density model, especially within the middle and lower sediment layers.

Whereas the mantle gravity pattern over West Antarctica revealed a relatively complex uppermost mantle structure, the gravity pattern over most of East Antarctica is much more uniform, indicating a relatively homogenous structure. We note that according to the lithospheric thickness model presented by Conrad and Lithgow-Bertelloni (2006), the lithosphere in East Antarctica deepens down to about 150–200 km, while the lithospheric thickness of West Antarctica is roughly 100 km. This thickness of the continental lithosphere is very similar to a maximum thickness of the oceanic lithosphere, while the maximum thickness of the continental lithosphere reaches globally 270 km (Conrad and Lithgow-Bertelloni 2006). The continental lithosphere may feature even larger variations in thickness, including continental roots that may penetrate to depths as much as 400 km beneath cratonic shields (e.g., Ritsema et al. 1999), and are likely cold and highly viscous.

More localized gravity lows in the mantle gravity map also agree with hotspot locations and volcanic provinces, particularly at the Balleny Islands (in the southern Indian Ocean), Mt. Erebus with possible extension under the Ross Island and Mt. Byrd, and Mt. Terror basaltic shield volcanoes (cf. Kiele et al. 1983). In addition, our result indicates a possible hotspot location that coincides with the South Orkney Islands (approximately 600 km northeast of the Antarctic Peninsula). This structure is a large part of continental fragments that form the South Scotia Ridge, and was separated from the Antarctic Peninsula probably during the Eocene and the Early Oligocene and reached its current position probably during the early Miocene (e.g., Dalziel and Elliot

1982; Dalziel 1992; Cande et al. 2000). The hotspot and continental crustal extension could explain the absence of orogenic roots for the Antarctic Peninsula.

Except for elongated gravity lows along the continental shelf of East Antarctica, the pronounced contrast between the continental and oceanic crust seen in the Bouguer gravity map (Fig. 5) is almost absent in the mantle gravity map. If this gravity pattern is not an artifact due to uncertainties of the used crustal density model, it might be explained as a possible signature of the isostatically uncompensated lithosphere due to ice load. In other words, when removing the ice mass, these gravity lows will disappear after the relaxation of the lithosphere. Obviously, this hypothesis could only be verified by modeling the response of the lithosphere on the removal of glacier cover in East Antarctica.

6. Summary and Concluding Remarks

We have compiled gravity maps for Antarctica based on the latest datasets of the gravity, topography, bathymetry, subglacial relief, sediment and crystalline crustal density structures, and Moho geometry. We then used these gravity maps to interpret the gravity pattern in the context of major known tectonic and geological features.

We have demonstrated that the free-air gravity field over Antarctica varies at a relatively small interval, thus indicating that most of the long–medium topographic features and lithospheric structural heterogeneities are isostatically compensated. The current rates of the gravity change in Antarctica due to the ice loss or ice accumulation are relatively small, locally reaching (or slightly exceeding) about 10 μGal/year. Gravity changes due to the glacial isostatic adjustment mainly attributed to the Late Pleistocene deglaciation are even smaller. Riva et al. (2009), for instance, estimated that the glacial isostatic adjustment in Antarctica reaches maxima to about 1 cm/year, corresponding to a gravity change of about 2 μGal/year. Such gravity changes, thus, have no influence on a gravimetric interpretation, but some features in the Bouguer and mantle gravity maps along the Antarctic continental margins suggest a possible relation with the ongoing lithospheric and

mantle relaxation after the Late Pleistocene deglaciation.

The Bouguer gravity map revealed detailed crustal thickness variations. The contrast between different thickness of the continental and oceanic crust propagates into the gravity pattern by large horizontal gravity changes along continental margins. This information provides more realistic interpretation of the Antarctic continental extension than that inferred based on the bathymetric depth detection directly from echo-sonars or indirectly from gravity data inversion, especially in the case of permanent sea ice cover. This is because the ocean floor relief indicates only locations of the continental slope, but not the geometry of the continental lithosphere located deeper under the ocean floor. The Bouguer gravity map also shows the isostatic signature of relatively compact orogenic roots under the Gamburtsev Subglacial Mountains and a complex orogenic structure under the Dronning Maud Land, consisting of two distinctive orogenic roots under the Kottas Mountains and the Wohlthat massif. A possible presence of additional orogenic fragments in that region is open for further investigation.

The mantle gravity map revealed the gravitational signature of divergent tectonic margins along the mid-oceanic rift zones surrounding the Antarctic tectonic plate and connected with the West Antarctic Rift System. Moreover, this gravity pattern indicates the possible existence of two continental rift segments. The west (continental margin) segment comprises faults and volcanoes along the continental margins of the Marie Byrd Land and the Antarctic Peninsula. The east (continental) segment separates the Ross Sea Shelf and the Bentley depression from the Transantarctic Mountains and the Ellsworth-Whitmore Mountains, and then continues approximately between the Antarctic Peninsula and the Filchner-Ronne Ice Shelf. The mantle gravity map further confirmed the complex tectonic structure of West Antarctica in contrast to a more homogenous, old, and stable formation of the East Antarctic Craton. This is evident from large gravity variations over West Antarctica and a smooth gravity pattern over East Antarctica. The mantle gravity variations over the entire study area are roughly within 1000 mGal, and comprise not only the gravitational signal

attributed to the uppermost mantle structure, but reflect also the long-wavelength gravity signature of a deep mantle convection pattern. Without the knowledge about the mantle density distribution, however, the separation of these two gravity signals is not unique, because the long-wavelength gravity spectrum comprises both these gravitational contributions.

In addition to the gravitational signature of the divergent tectonic boundaries, the gravity minima mark known hotspots and volcanic regions. Moreover, our results indicate the possible existence of a hotspot under the South Orkney Island, and likely more complex systems of volcanos for the West Antarctic Rift System along the Transantarctic Mountains and the Marie Byrd Land. These findings, obviously, need to be further verified using seismic and/or magnetic surveys.

References

Accardo, N. J., s, D. A., Hernandez, S., Aster, R. C., Nyblade, A., Huerta, A., et al. (2014). Upper mantle seismic anisotropy beneath the West Antarctic Rift System and surrounding region from shear wave splitting analysis. *Geophysical Journal International, 198,* 414–429.

Adams, R. D. (1971). Reflections from discontinuities beneath Antarctica. *Bulletin of the Seismological Society of America, 5,* 1441–1451.

Amante, C., Eakins, B.W. (2009) ETOPO1 1 arc-minute global relief model: Procedures, data sources and analysis. NOAA, Technical memorandum, NESDIS, NGDC-24, p. 19

An, M., Wiens, D. A., Zhao, Y., Feng, M., Nyblade, A. A., Kanao, M., et al. (2015). S-velocity model and inferred Moho topography beneath the Antarctic Plate from Rayleigh waves. *Journal of Geophysical Research: Solid Earth, 120,* 359–383.

Bamber, J. L., Ferraccioli, F., Joughin, I., Shepherd, T., Rippin, D. M., Sigert, M. J., et al. (2006). East Antarctic ice stream tributary underlain by major sedimentary basin. *Geology, 34*(1), 33–36.

Bannister, S., Yu, J., Leitner, B., & Kennett, B. L. N. (2003). Variations in crustal structure across the transition from West to East Antarctica Southern Victoria Land. *Geophysical Journal International, 155,* 870–884.

Baranov, A., & Morelli, A. (2013). The Moho depth map of the Antarctica region. *Tectonophys, 609,* 299–313.

Baranov, A., Tenzer, R., Bagherbandi, M. (2018) Combined gravimetric-seismic crustal model for Antarctica. *Surveys in Geophysics, 39*(1), 23–56.

Behrendt, J. C., LeMasurier, W. E., Cooper, A. K., Tessensohn, F., Trehu, A., & Damaske, D. (1991). Geophysical studies of the West Antarctic rift system. *Tectonics, 10*(6), 1257–1273.

Bentley, C. R., & Ostenso, N. A. (1962). On the paper of F.F. Evison, C.E. Ingram, R.H. Orr, and J.H. LeFort (1962),

Thickness of the Earth's crust in Antarctica and surrounding oceans. *Geophysical Journal of the Royal Astronomical Society, 6,* 292–298.

Bialas, R. W., Buck, W. R., Studinger, M., & Fitzgerald, P. (2007). Plateau collapse model for the Transantarctic Mountains West Antarctic Rift System: insights from numerical experiments. *Geology, 35*(8), 687–690.

Block, A. E., Bell, R. E., & Studinger, M. (2009). Antarctic crustal thickness from satellite gravity: implications for the Transantarctic and Gamburtsev Subglacial Mountains. *Earth and Planetary Science Letters, 288*(1–2), 194–203.

Cande, S. C., Stock, J. M., Müller, R. D., & Ishihara, T. (2000). Cenozoic motion between East and West Antarctica. *Nature, 404,* 145–150.

Chaput, J., Aster, R. C., Huerta, A., Sun, X., Lloyd, A., Wiens, D., et al. (2014). The crustal thickness of West Antarctica. *Journal of Geophysical Research: Solid Earth, 119,* 378–395. https://doi.org/10.1002/2013JB010642.

Chen, W., Tenzer, R., & Gu, X. (2014). Sediment stripping correction to marine gravity data. *Marine Geodesy, 37*(4), 419–439.

Conrad, C. P., & Lithgow-Bertelloni, C. (2006). Influence of continental roots and asthenosphere on plate-mantle coupling. *Geophysical Research Letters, 33,* L05312.

Cutnell, J. D., & Kenneth, W. J. (1995). *Physics* (3rd ed.). New York: Wiley.

Dalziel, I. W. D. (1992). Antarctica: a tale of two supercontinents. *Annual Review of Earth and Planetary Sciences, 20,* 501–526.

Dalziel, I. W. D., & Elliot, D. H. (1982). West Antarctica; problem child of Gondwanaland. *Tectonics, 1*(1), 3–19.

Dewart, G. M., & Toksoz, M. N. (1965). Crustal structure in East Antarctica from surface wave dispersion. *Journals-Royal Astronomical Society, 10,* 127–139.

Evison, F. F., Ingham, C. E., Orr, R. H., & Le Fort, J. H. (1960). Thickness of the earth's crust in Antarctica and the surrounding oceans. *Geophysical Journal, 3,* 289–306.

Fedorov, L. V., Grikurov, G. E., Kurinin, R. G., & Masolov, V. N. (1982). Crustal structure of the Lambert Glacier area from geophysical data. In C. Craddock (Ed.), *Antarctic Geoscience* (pp. 931–936). Madison: Univ. of Wisconsin Press.

Ferraccioli, F., Finn, C. A., Jordan, T. A., Bell, R. E., Anderson, L. M., & Damaske, D. (2011). East Antarctic rifting triggers uplift of the Gamburtsev Mountains. *Nature, 479,* 388–392.

Ferris, J., Johnson, A., & Storey, B. (1998). Form and extent of the Dufek intrusion, Antarctica, from newly compiled aeromagnetic data. *Earth and Planetary Science Letters, 154*(1–4), 185–202.

Forsyth, S. W., Ehrenbarda, R. L., & Chapin, S. (1987). Anomalous upper mantle beneath the Australian-Antarctic discordance. *Earth and Planetary Science Letters, 84,* 471–478.

Fretwell, P., Pritchard, H. D., Vaughan, D. G., Bamber, J. L., Barrand, N. E., Bell, R., et al. (2013). Bedmap2: improved ice bed, surface and thickness datasets for Antarctica. *The Cryosphere, 7,* 375–393.

Gladkikh, V., & Tenzer, R. (2011). A mathematical model of the global ocean saltwater density distribution. *Pure and Applied Geophysics, 169*(1–2), 249–257.

Groushinsky, A. N., Groushinsky, N. P., Stroev, P. A., & Yatsenko, E. V. (1992). The Earth's crust in Antarctica and the effective relief of the continent. *Journal of Geodynamics, 15,* 223–228.

Hansen, S., Nyblade, A., Pyle, M., Wiens, D., & Anandakrishnan, S. (2009). Using S wave receiver functions to estimate crustal structure beneath ice sheets: an application to the Transantarctic

Mountains and East Antarctic craton. *Geochemistry, Geophysics, Geosystems, 10,* Q08014.

Heiskanen, W. H., & Moritz, H. (1967). *Physical geodesy*. San Francisco: Freeman W.H.

Hinze, W. J. (2003). Bouguer reduction density, why 2.67? *Geophysics, 68*(5), 1559–1560.

Huebscher, C., Jokat, W., & Miller, H. (1996). Structure and origin of southern Weddell Sea crust: results and implications. In B. C. Storey, E. C. King, & R. A. Livermore (Eds.), *Weddell Sea Tectonics and Gondwana Break-up: Geological Society*. London: Geological Society of London.

Ito, K., & Ikami, A. (1986). Crustal structure of the Mizuho Plateau, East Antarctica, from geophysical data. *Journal of Geodynamics, 6,* 285–296.

Jacobs, J., Bauer, W., & Fanning, C. M. (2003). Late Neoproterozoic/Early Palaeozoic events in central Dronning Maud Land and significance for the southern extension of the East African Orogen into East Antarctica. *Precambrian Research, 126,* 27–53.

Jacobs, J., Elburg, M., Läufer, A. L., Kleinhanns, I. C., Henjes-Kunst, F., Estrada, S., et al. (2015). Two distinct Late Mesoproterozoic/Early Neoproterozoic basement provinces in central/eastern Dronning Maud Land, East Antarctica: the missing link, 15–21E. *Precambrian Research, 265,* 249–272.

Jacobs, J., Fanning, C. M., Henjes-Kunst, F., Olesch, M., & Paech, H. J. (1998). Continuation of the Mozambique Belt into East Antarctica: Grenville-age metamorphism and polyphase Pan-African high-grade events in central Dronning Maud Land. *The Journal of Geology, 106*(4), 385–406.

Jordan, T. A., Ferraccioli, F., Armadillo, E., & Bozzo, E. (2013). Crustal architecture of the Wilkes Subglacial Basin in East Antarctica, as revealed from airborne gravity data. *Tectonophysics, 585,* 196–206.

Jordan, T. A., Ferraccioli, F., Vaughan, D. G., Holt, J. W., Corr, H., Blankenship, D. D., et al. (2010). Aerogravity evidence for major crustal thinning under the Pine Island Glacier region (West Antarctica). *Geological Society of America Bulletin, 122,* 714–726.

Kiele, J., Marshall, D. L., Kyle, P. R., Kaminuma, K., Shibuya, K., & Dibble, R. R. (1983). Volcanic activity associated and seismicity of Mount Erebus 1982–1983. *Antarctica JUS, 18,* 41–44.

Knopoff, L., & Vane, G. (1978). Age of East Antarctica from surface wave dispersion. *Pure and Applied Geophysics, 117,* 806–816.

Kogan, A. L. (1972). Results of deep seismic soundings of the earth's crust in East Antarctica. In R. J. Adie (Ed.), *Antarctic geology and geophysics* (pp. 485–489). Oslo: Universitetsforlag.

Kolmakov, A.F., Mishenkin, B.P., Solovyev, D.S. (1975) Deep seismic studies in East Antarctica. *Bulletin Soviet Antarctic Expedition*, 5–15 (in Russian)

Kovach, R. L., & Press, F. (1961). Surface wave dispersion and crustal structure in Antarctica and the surrounding oceans. *Annali di Geofisica, 14,* 211–224.

Laske, G., Masters, G., Ma, Z., & Pasyanos, M. E. (2013). Update on CRUST1.0—A 1-degree global model of Earth's crust. *Geophysical Research Abstracts, 15,* 2658.

Lawrence, J.F., van Wijk, J.W., Driscoll, N.W. (2007) Tectonic implications for uplift of the Transantarctic Mountains" (PDF), USGS. In: 10th International Symposium on Antarctic Earth Sciences.

Lawrence, J. F., Wiens, D. A., Nyblade, A., Anandakrishnan, S., Shore, P. J., & Voigt, D. (2006). *Crust and upper mantle*

structure of the Transantarctic Mountains and surrounding regions from receiver functions, surface waves, and gravity: implications for uplift models (p. 7). Geosyst: Geochemistry, Geophysics.

Leitchenkov, G., & Kudryavtzev, G. (1997). Structure and origin of the Earth's Crust in the Weddell Sea Embayment (beneath the Front of the Filehner and Ronne Ice Shelves) from deep seismic sounding data. Polarforschung, 67(3), 143–154.

Lloyd, A. J., Wiens, D. A., Nyblade, A. A., Anandakrishnan, S., Aster, R. C., Huerta, A. D., et al. (2015). A seismic transect across West Antarctica: Evidence for mantle thermal anomalies beneath the Bentley Subglacial Trench and the Marie Byrd Land Dome. Journal of Geophysical Research: Solid Earth, 120(12), 2169–9356.

Llubes, M., Florsch, N., Legresy, B., Lemoine, J. M., Loyer, S., Crossley, D., et al. (2003). Crustal thickness in Antarctica from CHAMP gravimetry. Earth and Planetary Science Letters, 212, 103–117.

Marschall, H. R., Hawkesworth, C., & Leat, P. T. (2013). Meso-proterozoic subduction under the eastern edge of the Kalahari-Grunehogna Craton preceding Rodinia assembly: the Ritscher-flya detrital zircon record, Ahlmannryggen (Dronning MaudLand, Antarctica). Precambrian Research, 236, 31–45.

Mayer-Gürr, T., Pail, R., Gruber, T., Fecher, T., Rexer, M., Schuh, W.-D., Kusche, J., Brockmann, J.-M., Rieser, D., Zehentner, N., Kvas A., Klinger, B., Baur, O., Höck, E., Krauss, S., Jäggi, A. (2015) The combined satellite gravity field model GOCO05s. Presentation at EGU 2015, Vienna, April 2015

Mieth, M., & Jokat, W. (2014). New aeromagnetic view of the geological fabric of southern Dronning Maud Land and Coats Land, East Antarctica. Gondwana Research, 25, 358–367.

Molinari, I., & Morelli, A. (2011). EPcrust: a reference crustal model for the European Plate. Geophysical Journal International, 185, 352–364.

Morelli, A., & Danesi, S. (2004). Seismological imaging of the Antarctic continental lithosphere: a review. Global and Planetary Change, 42, 155–165.

Moritz, H. (2000). Geodetic Reference System 1980. Journal of Geodesy, 74, 128162.

O'Donnell, J. P., & Nyblade, A. A. (2014). Antarctica's hypsometry and crustal thickness: implications for the origin of anomalous topography in East Antarctica. Earth and Planetary Science Letters, 388, 143–155.

Okal, E. A. (1981). Intraplate seismicity of Antarctica and tectonic implications. Earth and Planetary Science Letters, 52, 397–409.

Ramirez, C., Nyblade, A., Hansen, S. E., Wiens, D. A., Anandakrishnan, S., Aster, R. C., et al. (2016). Crustal and upper-mantle structure beneath ice-covered regions in Antarctica from S-wave receiver functions and implications for heat flow. Geophysical Journal International, 204, 1636–1648.

Reading, A. M. (2006). The seismic structure of Precambrian and early Paleozoic terranes in the Lambert Glacier region East Antarctica. Earth and Planetary Science Letters, 244, 44–57.

Ritsema, J., van Heijst, J. J., & Woodhouse, J. H. (1999). Complex shear wave velocity structure imaged beneath Africa and Iceland. Science, 286, 1925–1928.

Ritzwoller, M. H., Shapiro, N. M., Levshin, A. L., & Leahy, G. M. (2001). Crustal and upper mantle structure beneath Antarctica and surrounding oceans. Journal of Geophysical Research, B, 106(12), 30645–30670.

Riva, R. E. M., Gunter, B. C., Urban, T. J., Vermeersen, B. L. A., Lindenbergh, R. C., Helsen, M. M., et al. (2009). Glacial isostatic adjustment over antarctica from combined icesat and grace satellite data. Earth and Planetary Science Letters, 288, 516–523.

Rooney, S. T., Blankenship, D. D., & Bentley, C. R. (1987). Seismic refraction measurements of crustal structure in West Antarctica. In G. D. McKenzie (Ed.), Gondwana six: structure, tectonics and geophysics. geophysical monograph series (40th ed., pp. 1–7). Washington: American Geophysical Union.

Rouland, D., Xu, S. H., & Schindele, F. (1985). Upper mantle structure in the southeast Indian Ocean: a surface wave investigation. Tectonophys, 114, 281–292.

Roult, G., Rouland, D., & Montagner, J. P. (1994). Antarctica II: upper mantle structure from velocities and anisotropy. Physics of the Earth and Planetary Interiors, 84, 33–57.

Stern, T. A., & ten Brink, U. S. (1989). Flexural uplift of the Transantarctic Mountains. Journal of Geophysical Research, 94, 10315–10330.

Studinger, M., Bell, R. E., Buck, W. R., Karner, G. D., & Blankenship, D. (2004). Sub-ice geology inland of the Transantarctic Mountains in light of new aerogeophysical data. Earth and Planetary Science Letters, 220(3–4), 391–408.

Studinger, M., Bell, R. E., Fitzgerald, P., & Buck, W. R. (2006). Crustal architecture of the Transantarctic Mountains between the Scott and Reedy Glacier region and South Pole from aero-geo-physical data. Earth and Planetary Science Letters, 250(1–2), 182–199.

Studinger, M., Karner, G. D., Bell, R. E., Levin, V., Raymond, C. A., & Tikku, A. A. (2003). Geophysical models for the tectonic framework of the Lake Vostok region East Antarctica. Earth and Planetary Science Letters, 216(4), 663–677.

ten Brink, U. S., Hackney, R. I., Bannister, S., Stern, T., & Makovsky, Y. (1997). Uplift of the Transantarctic Mountains and the bedrock beneath the East Antarctic ice sheet. Journal of Geophysical Research, B, 12, 27603–27621.

Tenzer, R., Abdalla, A., & Vajda, P. (2010). The spherical harmonic representation of the gravitational field quantities generated by the ice density contrast. Contributions to Geophysics and Geodesy, 40(3), 207–223.

Tenzer, R., Bagherbandi, M., Chen, W., & Sjöberg, L. E. (2016). Global isostatic gravity maps from satellite missions and their applications in the lithospheric structure studies. IEEE Journal of Selected Topics in Applied Earth Observations and Remote Sensing, 10(2), 549–561.

Tenzer, R., Bagherbandi, M., & Gladkikh, V. (2012a). Signature of the upper mantle density structure in the refined gravity data. Computational Geosciences, 16(4), 975–986.

Tenzer, R., Chen, W., & Jin, S. (2015a). Effect of the upper mantle density structure on the Moho geometry. Pure and Applied Geophysics, 172(6), 1563–1583.

Tenzer, R., Chen, W., Tsoulis, D., Bagherbandi, M., Sjöberg, L. E., Novák, P., et al. (2015b). Analysis of the refined CRUST1.0 crustal model and its gravity field. Surveys In Geophysics, 36(1), 139–165.

Tenzer, R., Chen, W., & Ye, Z. (2015c). Empirical model of the gravitational field generated by the oceanic lithosphere. Advances in Space Research, 55(1), 72–82.

Tenzer, R., & Gladkikh, V. (2014). Assessment of density variations of marine sediments with ocean and sediment depths. Scientific World Journal, 823296, 9.

Tenzer, R., Gladkikh, V., Vajda, P., & Novák, P. (2012b). Spatial and spectral analysis of refined gravity data for modelling the crust-mantle interface and mantle-lithosphere structure. *Surveys In Geophysics, 33*(5), 817–839.

Tenzer, R., Novák, P., & Gladkikh, V. (2011). On the accuracy of the bathymetry-generated gravitational field quantities for a depth-dependent seawater density distribution. *Studia Geophysica et Geodaetica, 55*(4), 609–626.

Tenzer, R., Novák, P., & Gladkikh, V. (2012c). The bathymetric stripping corrections to gravity field quantities for a depth-dependent model of the seawater density. *Marine Geodesy, 35,* 198–220.

Tenzer, R. H., Novák, P., Gladkikh, V., & Vajda, P. (2012d). Global crust-mantle density contrast estimated from EGM2008, DTM2008, CRUST2.0, and ICE-5G. *Pure and Applied Geophysics, 169*(9), 1663–1678.

Tenzer, R., Novák, P., Vajda, P., & Gladkikh, V. (2012e). Spectral harmonic analysis and synthesis of Earth's crust gravity field. *Computational Geosciences, 16*(1), 193–207.

Tenzer, R., Hamayun, K, & Vajda, P. (2009a). Global maps of the CRUST2.0 components stripped gravity disturbances. *Journal of Geophysical Research (Solid Earth), 114,* B05408.

Tenzer, R., Hamayun, K., & Vajda, P. (2009b). A global correlation of the step-wise consolidated crust-stripped gravity field quantities with the topography, bathymetry, and the CRUST 2.0 Moho boundary. *Contributions to Geophysics and Geodesy, 39*(2), 133–147.

Tenzer, R., Hamayun, K., & Vajda, P. (2009c). Global atmospheric corrections to the gravity field quantities. *Contributions to Geophysics and Geodesy, 39*(3), 221–236.

Trey, H., Cooper, A., Pellis, G., della Vedova, B., Cochrane, G., Brancolini, G., et al. (1999). Transect across the West Antarctic rift system in the Ross Sea. *Antarctica Tectonophys, 301,* 61–74.

von Frese, R. R. B., Tan, L., Kim, J. W., & Bentley, C. R. (1999). Antarctic crustal modeling from the spectral correlation of free-air gravity anomalies with the terrain. *Journal of Geophysical Research, 104,* 25275–25296.

Winberry, J. P., & Anandakrishnan, S. (2004). Crustal structure of the West Antarctic rift system and Marie Byrd Land hotspot. *Geology, 32,* 977–980.

Wright, R., & Anderson, J. B. (1982). The importance of sediment gravity flow to sediment transport and sorting in a glacial marine environment: Eastern Weddell Sea, Antarctica. *Bulletin of the Geological Society of America, 93*(10), 951–963.